Impact of 3D Channel Modeling for Ultra-High Speed Beyond-5G Networks

Sherif Adeshina Busari*, Kazi Mohammed Saidul Huq*, Shahid Mumtaz* and Jonathan Rodriguez*,‡
*Instituto de Telecomunicações, 3810-193, Aveiro, Portugal
‡University of South Wales, Pontypridd, CF37 1DL, United Kingdom
Email: {sherifbusari, kazi.saidul, smumtaz, jonathan}@av.it.pt; jonathan.rodriguez@southwales.ac.uk

***Abstract*—Three-dimensional (3D) channel models are essential for the accurate and realistic performance evaluation of mobile networks. Legacy 2D channel models have been shown to underestimate performance. Also, 5G/B5G systems will feature both microwave (μWave) and millimeter-wave (mmWave) channels. Using the 3GPP 3D channel models in these two frequency bands, we analyzed system performance in urban macrocell (UMa) and urban microcell (UMi) scenarios. Our results show that the mmWave tier anticipated to provide multi-gigabits-per-second throughputs suffers SINR bottleneck, particularly for indoor users served by outdoor base stations (BSs). The SINR statistics reveal that indoor users experience up to 30 dB additional losses from wall and in-building objects. It also reveals the degrading impact of the higher noise levels resulting from the larger bandwidths employed in mmWave systems. The impact of user height distribution and BS downtilt angles on system performance have also been investigated. To realize ultra-high speed networks, future 5G/B5G systems must employ techniques that will significantly enhance the SINR in order to optimize performance in the face of the limiting channel effects.**

***Index Terms*—3D propagation models, 3GPP channel models, 5G HetNets, microwave channels, mmWave channels, SINR.**

I. Introduction

The Third Generation Partnership Project (3GPP) has recently approved three broad categories of use cases: enhanced mobile broadband (eMBB), ultra-reliable and low-latency communications (URLLC) and massive machine type communications (mMTC). With these scenarios, the fifth-generation (5G) and beyond-5G (B5G) networks are expected to deliver speed, latency, reliability and connectivity that significantly surpass those of legacy networks [1]. In order to evaluate the performance of the networks, however, accurate characterization of the radio environment or the wireless channel is fundamental.

Over time, several channel models have evolved. These include the COST series (231, 259 and 273), the WINNER family (I and II), and the spatial channel models (SCMs), among others. Studies such as [2], [3], [4], among others, have shown that two-dimensional (2D) channel models underestimate the throughput performance. Three-dimensional (3D) channel models, therefore, give a more realistic outlook as they consider the elevation (zenith/vertical) angles alongside the azimuth (horizontal) angles used by the 2D models.

In addition, three significant paradigms are shifting interest away from the 2D microwave (μWave) channel models. The first paradigm is the growing interest in the millimeter wave (mmWave) bands with amazing spectral prospects. Elevation beamforming, enabled by mmWave massive multiple-input multiple-output (MIMO) and planar (2D) antenna arrays, constitutes the second paradigm. Interest in outdoor-to-indoor (O2I) and indoor-to-outdoor (I2O) propagation modeling that account for building, blockage and other limiting effects is the third [5], [6], [7].

Accordingly, newer channel models which address these interests have continued to evolve and they fundamentally result from extensive channel measurement campaigns [8]. These include the WINNER+, COST 2100 and 3GPP TR 36.873 models for 3D μWave channels, and the QuaDRiGa, MiWEBA, IEEE 802.11ad and 3GPP TR 38.900 models for the 3D mmWave channels, among others [9]. In this work, however, we consider the 3D 3GPP TR 36.873 (μWave) [5] and 3GPP TR 38.900 (mmWave) [6] channel models. The motivation is to investigate the performance of the two models and provide insights for 5G/B5G networks. Fortunately, these future networks are anticipated to be multi-tier, heterogeneous networks (HetNets) where the μWave tier will provide coverage and signaling while the mmWave tier provides the anticipated capacity boost [10].

Notably, 3D channel models account for a high volume of parameters, variables and dependencies. As a result, analyses of their performance require systematic investigation. Thus, we limit discussion to the path loss (PL) and shadow fading (SF) statistics. Analysis of the small-scale, fast-fading effects is left for future work. The key contributions of this paper are that: (i) we provide a comparison of the two channel models in urban macrocell (UMa) and urban microcell (UMi) scenarios, in the light of 5G HetNets; (ii) we adopt a map-based approach which gives a more representative statistics as compared to the conventional drop-based approach that is limited by the number of simulation runs; (iii) we assess performance using varied metrics that are useful not only for evaluation but also for channel calibration purposes; and (iv) we present simplified models with reduced number of variables useful for intuitive prediction of performance and as quick source of reference.

The remainder of this paper is organized as follows. In Section II, we present the system model detailing the network deployment, simulation parameters and algorithm. In Section III, simulation results are presented with a discussion of findings. Analysis of the results follows in Section IV. The conclusions and future works are presented in Section V.

II. System Model

In this section, we describe the considered network layout, outline the simulation parameters and present the algorithm for the map-based simulation framework employed. Except otherwise stated, we follow strictly the 3GPP-compliant baseline for evaluation in [5] and [6] for the sub-6 GHz μWave and above-6 GHz mmWave bands, respectively.

A. Network Deployment

We show in Fig. 1 the considered system layout. It is a square grid with 57 base stations (BSs) composed of 19 tri-sectored sites. The BSs are deployed based on the inter-site distance (ISD) of the respective scenarios. The considered area is further divided into $X \times Y$ smaller squares, on a 10:1 map resolution for complexity reduction. Users are deployed in the mapped area with a user equipment (UE) per small square. This corresponds, for example, to more than 50,000 UEs in the UMa scenario. The four scenarios considered in this work are the UMa and UMi scenarios for both the μWave [5] and the mmWave bands [6], as highlighted in Table I.

The simulation parameters employed are based on Tables (6.1, 7.1-1, 8.2-1 and 8.2-2) in [5] and Tables (7.2-1, 7.3-1, 7.8-1 and 7.8-2) in [6] for the μWave and mmWave bands, respectively. For all scenarios, the BSs have planar antenna arrays with 4×10 elements while the UEs have linear antenna arrays with 2×1 elements. All elements are spaced 0.5λ apart (where λ is the wavelength) along the horizontal and vertical, as the case may be. All antenna ports are co-polarized. Each element has a gain of 8 dBi with 102^o downtilt at the BS, and a gain of 0 dBi, 9 dB noise figure (NF) and -174 dBm/Hz thermal noise density (N_o) for the omnidirectional UEs. The scenario-specific parameters are further given in Table I, where f_c is the carrier frequency, P_{TX} is the transmit power, B is the bandwidth and h_{BS} is the BS height.

B. Map-based Simulation Framework

The simulation flow follows the framework in Algorithm 1 which outputs the reference signal received power (RSRP) for all users in the mapped area. It uses the parameters in Tables I - III to compute the PL and SF based on Tables 7.2-1 [5] and 7.4.1-1 [6] for the μWave and mmWave bands, respectively. SF is modeled as a distance-dependent log-normal distribution (0, σ), with zero mean and standard deviation (σ) following the Claussen implementation in [11], [12].

The transmit antenna gains (G_{TX}) are calculated based on Tables 7.1-1 [5] and 7.3-1 [6], for the μWave and mmWave, respectively. For each scenario, a UE may be in line-of-sight (LOS) or non-line-of-site (NLOS), in either outdoor-to-outdoor (O2O) or outdoor-to-indoor (O2I) environment to each BS, and the various UE maps (indoor distance (d_{2D-in}), outdoor distance (d_{2D-out}), height (h_{UE}), LOS probability (P_{LOS}), etc) are generated accordingly (see Algorithm 1 and note that we have used j and k to represent subscripts BS and UE, respectively).

TABLE I
KEY SIMULATION PARAMETERS

Parameters	UMa **μWave**	UMi **μWave**	UMa **mmWave**	UMi **mmWave**
f_c (GHz)	2		28	
P_{TX} (dBm)	46		35	
B (MHz)	10		125	
h_{BS} (m)	25	10	25	10
ISD (m)	500	200	500	200

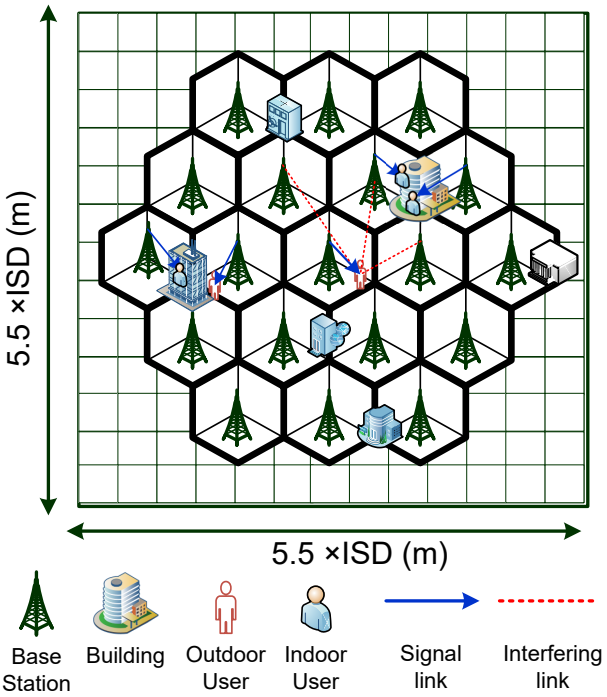

Fig. 1. Network deployment layout

In Table III, unlike in [5] and [6], we have plugged in all the constant parameters for the respective scenarios, leaving only f_c, d_{3D}, h_{UE} and the break-point distance (d_{BP}) variables. The values of these parameters depend on the state of the simulation with respect to the scenario and user location in each run and/or transmission time interval (TTI). For each scenario, 1000 simulation runs are performed and averaged. The empirical cumulative distribution function (ECDF) is used to analyze the results.

III. Simulation Results

In this section, we present the simulation results for the four scenarios considered using the coupling loss (CL), geometry factor (GF), signal to interference plus noise (SINR), signal-to-noise ratio (SNR), and signal-to-interference ratio (SIR) as performance metrics.

A. Coupling Loss

The difference between the received signal and the transmitted signal along the LOS direction is the coupling loss (CL) [2]. For each user and its attached BS, the CL (dB) and the RSRP (dB) are defined as (1) and (2), respectively.

Algorithm 1: Map-based simulation framework

Inputs :

$j = \{1, 2, ..., J\}$: Total number of BSs

$k = \{1, 2, ..., K\}$: Total number of UEs

$\{x_j, y_j\}, \{x_k, y_k\}$: 2D coordinates of BS and UE

P_{TX}^{j} : TX power per BS

Output:

$RSRP_k$: RSRP of each user

Steps

I - Generate UE indoor-outdoor map (80%-20%)

$\chi = \texttt{binornd}(1, 0.8, X, Y)$

$$\chi_k = \begin{cases} 0, & k \rightarrow \ outdoor \\ 1, & k \rightarrow \ indoor \end{cases}$$

II- Generate building floor map

$n_{fl}^{max} = \texttt{randi}([4, 8])$

$n_{fl} = \texttt{randi}(n_{fl}^{max}, X, Y)$

III- Generate indoor distance map

$d_{2D-in} = 25 \times \texttt{rand}(X, Y)$

for $k \rightarrow 1$ **to** K **do**

  IV- Compute UE height map

  $h_k = 1.5 + (\chi_k \times [3(n_{fl}^{k} - 1)])$

  for $j \rightarrow 1$ **to** J **do**

    V- Compute 2D & 3D distances to all BSs

    $d_{2D}^{k,j} = \sqrt{(x_j - x_k)^2 + (y_j - y_k)^2}$

    $d_{3D}^{k,j} = \sqrt{(d_{2D}^{k,j})^2 + (h_j - h_k)^2}$

    VI- Compute 2D outdoor distance map

    $d_{2D-out}^{k,j} = d_{2D}^{k,j} - (\chi_k \times d_{2D-in}^{k})$

    VII- Compute P_{LOS} using Table II

    $\xi_{k,j} = \texttt{binornd}(1, P_{LOS}^{k,j}(d_{2D-out}^{k,j}))$

$$\xi_{k,j} = \begin{cases} 0, & k, j \rightarrow \ NLOS \\ 1, & k, j \rightarrow \ LOS \end{cases}$$

    VIII- Compute $PL_{k,j}$ using Table III

$$\{\chi_k, \xi_{k,j}\} = \begin{cases} \{0,0\} & \rightarrow PL_{NLOS} \\ \{0,1\} & \rightarrow PL_{LOS} \\ \{1,0\} & \rightarrow PL_{O2I-NLOS} \\ \{1,1\} & \rightarrow PL_{O2I-LOS} \end{cases}$$

    IX- Compute $SF_{k,j}$ using Table III

    X- Compute $G_{TX}^{k,j}$ using [5], [6]; $G_{RX}^{k,j} = 0$

    XI- Compute $RSRP_{k,j}$

    $RSRP_{k,j} = P_{TX}^{k,j} + G_{TX}^{k,j} + G_{RX}^{k,j} - PL_{k,j} - SF_{k,j}$

  $RSRP_k = max(RSRP_{k,(1:J)})$

  Assign user $k \rightarrow j^{th}$ BS with $maxRSRP_k$

$$CL_k = RSRP_k - P_{TX}^{k,j} \quad (1)$$

$$RSRP_{k,j} = P_{TX}^{k,j} + G_{TX}^{k,j} + G_{RX}^{k,j} - PL_{k,j} - SF_{k,j} \quad (2)$$

CL depends only on the slow fading parameters. It captures all attenuation sources between a UE and its attached BS. As can be observed from (1) and (2), CL is independent of P_{TX} [13]. It is used in the Phase 1 calibration by standardization bodies such as 3GPP to bring companies and organizations involved in channel measurements and modeling to a common ground with respect to reported channel results [2].

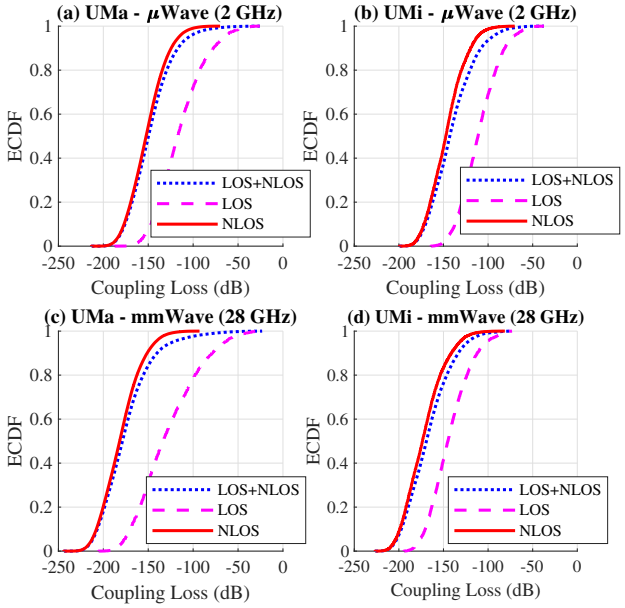

Fig. 2. Coupling Losses for the four scenarios

In Fig. 2, we show results for CL (i.e., the LOS curves) for the four scenarios. The minimum CL is 45 dB for both μWave UMa and UMi, and 35 dB and 75 dB for mmWave UMa and UMi, respectively. The results in Fig. 2(a) and (b) are consistent with [5], and Fig. 2(d) is consistent with the corresponding case in [13]. Further in Figs. 2(a)-(d), we provide loss curves for the NLOS UEs and the overall loss curves involving all UEs (both LOS and NLOS UEs combined). A penalty of around 20-35 dB is observed between the LOS and NLOS cases for the μWave band and around 20-50 dB for the mmWave case.

B. Geometry Factor

Geometry Factor (GF) captures the statistics of the SINR [13] or SIR [2] or either of the two [6]. These are necessary in order to compute the spectral efficiency (SE), UE throughput and cell capacity. The SINR, SIR and SNR for a given UE are defined as (3), (4) and (5), respectively.

$$SINR_k = RSRP_{k,j} - (\sum_{j=1,\ k \neq j}^{J} RSRP_{k,j} + N_k) \quad (3)$$

TABLE II
LOS PROBABILITY

Scenario	LOS Probability
UMa-μWave	$P_{LOS} = \left(\min\left(\frac{18}{d_{2D}}, 1\right)\left(1 - \exp\left(\frac{-d_{2D}}{63}\right)\right) + \exp\left(\frac{-d_{2D}}{63}\right)\right)\left(1 + C\left(d_{2D,h_{UE}}\right)\right)$
UMi-μWave	$P_{LOS} = \left(\min\left(\frac{18}{d_{2D}}, 1\right)\left(1 - \exp\left(\frac{-d_{2D}}{36}\right)\right) + \exp\left(\frac{-d_{2D}}{36}\right)\right)$
UMa-mmWave	$P_{LOS} = \begin{cases} 1, & d_{2D} \leq 18 \\ \left(\frac{18}{d_{2D}} + \exp\left(\frac{-d_{2D}}{63}\right)\left(1 - \frac{18}{d_{2D}}\right)\right)\left(1 + C\left(d_{2D,h_{UE}}\right)\right), & 18 < d_{2D} \end{cases}$
UMi-mmWave	$P_{LOS} = \begin{cases} 1, & d_{2D} \leq 18 \\ \left(\frac{18}{d_{2D}} + \exp\left(\frac{-d_{2D}}{36}\right)\left(1 - \frac{18}{d_{2D}}\right)\right), & 18 < d_{2D} \end{cases}$
where:	$C\left(d_{2D}, h_{UE}\right) = \begin{cases} 1, & d_{2D} \leq 18 \\ 1 + 1.25C'\left(h_{UE}\right)\left(\frac{d_{2D}}{100}\right)^3 \exp\left(\frac{-d_{2D}}{150}\right), & 18 < d_{2D} \end{cases}$
	$C'\left(h_{UE}\right) = \begin{cases} 0, & h_{UE} \leq 13 \\ \left(\frac{h_{UE} - 13}{10}\right)^{1.5}, & 13 < h_{UE} \leq 23 \end{cases}$
and	d_{2D} (which is d_{2D-out} in Algorithm 1) and h_{UE} are in meters (m) [5], [6]

TABLE III
PATHLOSS MODELS

Scenario	Pathloss (dB)	σ_{SF} (dB)
UMa-μWave	$PL_{LOS} = \begin{cases} 28 + 22\log_{10}(d_{3D}) + 20\log_{10}(f_c), & 10 < d_{2D} < d_{BP} \\ 28 + 40\log_{10}(d_{3D}) + 20\log_{10}(f_c) - 9\log_{10}((d_{BP})^2 + (25 - h_{UE})^2), & d_{BP} < d_{2D} < 5000 \end{cases}$	4
	$PL_{NLOS} = 69.51 + 39.09\log_{10}(d_{3D}) + 20\log_{10}(f_c) + 7.5\log_{10}(h_{UE}) - 0.6h_{UE} - 0.0825(h_{UE})^2$	6
	$PL_{O2I} = PL_{LOS/NLOS} + 20 + 0.5(d_{2D-in})$	7
UMi-μWave	$PL_{LOS} = \begin{cases} 28 + 22\log_{10}(d_{3D}) + 20\log_{10}(f_c), & 10 < d_{2D} < d_{BP} \\ 28 + 40\log_{10}(d_{3D}) + 20\log_{10}(f_c) - 9\log_{10}((d_{BP})^2 + (10 - h_{UE})^2), & d_{BP} < d_{2D} < 5000 \end{cases}$	3
	$PL_{NLOS} = 23.15 + 36.7\log_{10}(d_{3D}) + 26\log_{10}(f_c) - 0.3h_{UE}$	4
	$PL_{O2I} = PL_{LOS/NLOS} + 20 + 0.5(d_{2D-in})$	7
UMa-mmWave	$PL_{LOS} = \begin{cases} 32.4 + 20\log_{10}(d_{3D}) + 20\log_{10}(f_c), & 10 < d_{2D} < d_{BP} \\ 32.4 + 40\log_{10}(d_{3D}) + 20\log_{10}(f_c) - 10\log_{10}((d_{BP})^2 + (25 - h_{UE})^2), & d_{BP} < d_{2D} < 5000 \end{cases}$	4
	$PL_{NLOS} = 14.44 + 39.08\log_{10}(d_{3D}) + 20\log_{10}(f_c) - 0.6h_{UE}$	6
	$PL_{O2I} = PL_{LOS/NLOS} + PL_{wall} + 0.5(d_{2D-in})$	7
UMi-mmWave	$PL_{LOS} = \begin{cases} 32.4 + 21\log_{10}(d_{3D}) + 20\log_{10}(f_c), & 10 < d_{2D} < d_{BP} \\ 32.4 + 40\log_{10}(d_{3D}) + 20\log_{10}(f_c) - 9.5\log_{10}((d_{BP})^2 + (10 - h_{UE})^2), & d_{BP} < d_{2D} < 5000 \end{cases}$	4
	$PL_{NLOS} = 22.85 + 35.3\log_{10}(d_{3D}) + 21.3\log_{10}(f_c) - 0.3h_{UE}$	7.82
	$PL_{O2I} = PL_{LOS/NLOS} + PL_{wall} + 0.5(d_{2D-in})$	7
NOTES: f_c is in GHz; d_{2D}, d_{3D} and h_{UE} are in meters; $d_{BP} = 320((h_{UE} - 1)f_c)$ for UMa and $d_{BP} = 120((h_{UE} - 1)f_c)$ for UMi. d_{BP} is the break-point distance [5], [6] and PL_{wall} is the wall/penetration loss based on Tables 7.4.3-(1 & 2) in [6].		

$$SIR_k = RSRP_{k,j} - (\sum_{j=1,\ k \not\to j}^{J} RSRP_{k,j}) \quad (4)$$

$$SNR_k = RSRP_{k,j} - N_k \quad (5)$$

$$N_k = N_o + 10\log_{10} B_k + NF \quad (6)$$

GF measures the performance of users with respect to the received signal strength relative to the interference from other BSs (as SINR (with noise) or SIR (without noise)). It is used also in Phase 1 calibration to assess performance as a measure of UEs' SE and throughput [2]. The SNR performance, on the other hand, characterizes the maximum achievable capacity in interference-free scenarios [9].

The SNR/SIR/SINR performance for the four scenarios are shown in Fig. 3. In all cases, the SINR curves expectedly characterize the worst-case performance as they incorporate both the noise and interference terms. The SIR curves in Figs. 3(a) and (b) overlap the SINR curves, for the μWave UMa and μWave UMi scenarios, respectively. This outcome shows that μWave network is interference-limited. As for the mmWave scenarios, it is the SNR curves that overlap the SINR curves as shown in Figs. 3(c) and (d), for mmWave UMa and mmWave UMi cases, respectively. It reveals that the mmWave network is noise-limited for the considered scenario. However, for ultra-dense mmWave network with much shorter ISDs, the mmWave network could be interference-limited also due to transition from NLOS to LOS interference [14].

For all scenarios, GF follows a similar trend consistent with the results in [2] and [5] for the μWave scenarios, and [13] for the mmWave bands. In comparing the SNR/SIR/SINR

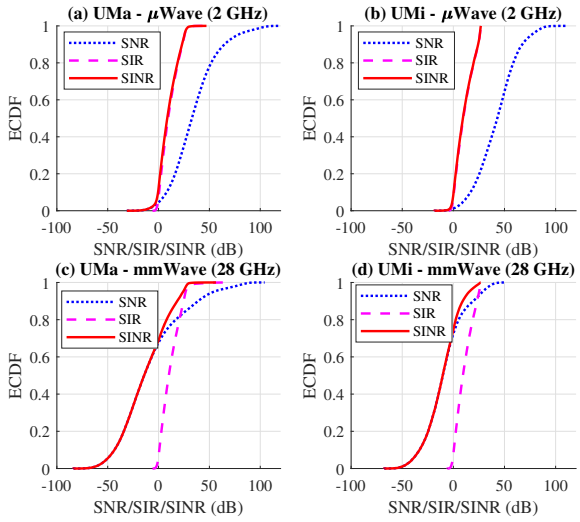

Fig. 3. Geometry Factor for the four scenarios

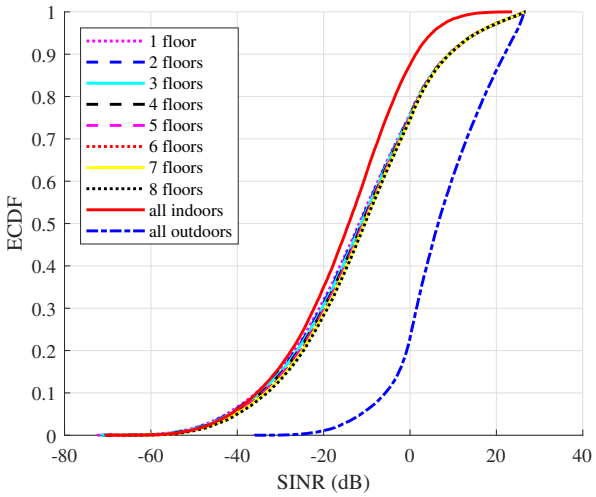

Fig. 4. Impact of UE height (floor level) on SINR

performance for the four scenarios, we use the 0 dB point which translates to an SE of 1 bps/Hz. The point where the ECDF curve first crosses the 0 dB point gives the percentage of users that will achieve an SE of 1 bps/Hz or less. For SNR, $\{4.5, 1.3, 68.9, 72.5\}$% of users achieve up to 0 dB (or SE of 1 bps/Hz) for the UMa-μWave, UMi-μWave, UMa-mmWave and UMi-mmWave scenarios, respectively. Therefore, while more than 95% of μWave users achieve SE greater than 1 bps/Hz in the μWave networks, only $\sim$30% of mmWave users will achieve the same feat.

As for SIR, $\{7.1, 8.8, 6.4, 7.6\}$% of users achieve up to 0 dB while in terms of SINR, $\{12.0, 8.9, 68.4, 74.6\}$% of users achieve up to 0 dB, for the same order in scenario. Again, mmWave systems perform poorly with only $\sim$30% of users achieving the 1 bps/Hz SINR, compared to $\sim$90% in the μWave set-ups. This SINR bottleneck is of grave concern for mmWave networks expected to provide the much-anticipated multi-gigabits-per-second throughputs in 5G/B5G networks. The results shown here are with 125 MHz mmWave bandwidth, based on [15], as 100 MHz is projected as the practical size for a component carrier in mmWave systems [16]. SINR degradation will therefore be of more significant consequences if much larger mmWave bandwidths (up to 1-2 GHz) are used, due to the expected increase in noise with increasing bandwidth as can be seen from (6).

IV. Analysis for 5G HetNets

Next-generation mobile networks (NGMNs) are foreseen to be multi-tier and multi-band. Legacy μWave macrocells will be overlaid with ultra-dense small cell networks (UDNs) operating on mmWave (and/or terahertz (THz)) frequency bands [1], [10]. This is aimed at reaping massive gains from high frequency-reuse and abundant available bandwidth, from UDNs and mmWave communications, respectively [17], [18]. 5G HetNets will thus feature UMa-μWave and UMi-mmWave channels. The μWave macrocells are expected to provide coverage. Low data rate from such cells are acceptable and the research on them is more established. On the other hand, the UMi-mmWave tier is foreseen to provide the much-anticipated capacity to meet the explosive data rate demands projected for the 5G/B5G era.

In this section, we investigate further the factors responsible for low SINR in 3D UMi channels. In Fig. 4, we show the effect of wall/penetration losses and indoor losses on the SINR performance. The two extremes are the cases when all UEs are indoors and when all UEs are outdoors. For the other cases, 20% of UEs are outdoors while the remaining 80% users which are indoors are randomly distributed according to the maximum number of floors. For example, the curve named "3 floors" means that the 80% indoor users are randomly distributed in floors 1-3, the curve named "7 floors" means that the 80% indoor users are randomly distributed in floors 1-7, and so on.

A significant 20-30 dB gap exists between when all the UEs are outdoors and when they are all indoors. Further, in the 3GPP's case with 20% of UEs outdoors and 80% indoors, the distribution of the indoor UEs across floors (i.e., the effect of UE heights) does not amount to significant impact on average performance. The differences are paled by the high number of UEs at system-level.

Further, we show in Fig. 5 the results of simulations for the two extreme cases only (i.e., all UEs indoors and all UEs outdoors) with different BS downtilt angles. Our results show that the downtilt angle does not significantly impact average performance. The observable gap between when all UEs are outdoors and when all UEs are indoors is attributable, again, to the wall and indoor losses. On aggregate, our results indicate that outdoor users show promising performance in mmWave 3D channels. On the other hand, the additional wall and indoor losses (on top of the inherently high path loss at mmWave frequencies) significantly degrade the performance of indoor users served by outdoor BSs. Therefore, overcoming

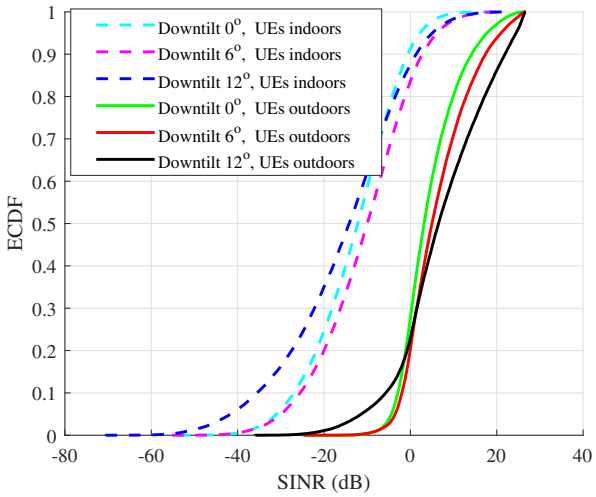

Fig. 5. Impact of BS downtilt angle on SINR

the collective impact of the increasing noise, higher pathloss and indoor losses remains a challenge for indoor users in the mmWave tier of 5G HetNets where high rates are anticipated.

V. Conclusion and Future Work

In this paper, we have presented the performance of 3D μWave and mmWave channel models for UMa and UMi scenarios. We employed 3GPP-compliant simulations to compare the performance of these models using varied metrics. Further, we analyzed the performance of the models in the light of 5G HetNets, with major highlight on the mmWave-UMi scenario. Our results show mmWave systems have higher coupling losses than μWave systems. The results also show that μWave systems are interference-limited while mmWave systems are noise-limited for the considered scenarios.

Also, indoor users served by outdoor BSs show highly degraded performance. This is due to the additional 20-30 dB wall and indoor losses experienced by indoor users. The degradation will become even more pronounced if much larger mmWave bandwidths are employed due to the expected increase in noise. As very high data rates are anticipated in mmWave small cell networks (corresponding to mmWave-UMi scenario) in NGMNs, techniques that will enhance the SINR of the systems are highly essential in exploiting the amazing spectral prospects at the mmWave frequencies. The analysis herein has been limited to large scale fading. Extension to the small-scale fading effects is our next direction for future work.

Acknowledgment

Sherif Busari and Kazi Huq would like to acknowledge their PhD and Post-doc grants funded by the Fundação para a Ciência e a Tecnologia (FCT-Portugal) with reference nos. PD/BD/113823/2015 and SFRH/BPD/110104/2015, respectively. Also, the research leading to these results received funding from the European Commission H2020 program under grant agreement no. 815178 (5GENESIS project).

References

[1] S. A. Busari, S. Mumtaz, S. Al-Rubaye, and J. Rodriguez, "5G Millimeter-Wave Mobile Broadband: Performance and Challenges," *IEEE Communications Magazine*, vol. 56, no. 6, pp. 137–143, June 2018.

[2] A. Kammoun, H. Khanfir, Z. Altman, M. Debbah, and M. Kamoun, "Preliminary Results on 3D Channel Modeling: From Theory to Standardization," *IEEE Journal on Selected Areas in Communications*, vol. 32, no. 6, pp. 1219–1229, June 2014.

[3] F. Ademaj, M. Taranetz, and M. Rupp, "3GPP 3D MIMO channel model: a holistic implementation guideline for open source simulation tools," *EURASIP Journal on Wireless Communications and Networking*, vol. 2016, no. 1, p. 55, Feb 2016.

[4] R. N. Almesaeed, A. S. Ameen, E. Mellios, A. Doufexi, and A. Nix, "3D Channel Models: Principles, Characteristics, and System Implications," *IEEE Communications Magazine*, vol. 55, no. 4, pp. 152–159, April 2017.

[5] "Study on 3D channel model for LTE, v12.2.0 , 3GPP TR 36.873," 3GPP, Tech. Rep., 2014, accessed Sep. 13, 2018. [Online]. Available: http://www.3gpp.org/ftp//Specs/archive/36_series/36.873

[6] "Study on channel model for frequency spectrum above 6 GHz, v14.2.0, 3GPP TR 38.900," 3GPP, Tech. Rep., 2016, accessed Sep. 13, 2018. [Online]. Available: http://www.3gpp.org/ftp//Specs/archive/38_series/38.900

[7] B. Ai, K. Guan, R. He, J. Li, G. Li, D. He, Z. Zhong, and K. M. S. Huq, "On Indoor Millimeter Wave Massive MIMO Channels: Measurement and Simulation," *IEEE Journal on Selected Areas in Communications*, vol. 35, no. 7, pp. 1678–1690, July 2017.

[8] S. A. Busari, S. Mumtaz, K. M. S. Huq, and J. Rodriguez, *Millimeter Wave Channel Measure*. Cham: Springer International Publishing, 2018, pp. 1–5. [Online]. Available: https://doi.org/10.1007/978-3-319-32903-1_115-1

[9] M. Xiao, S. Mumtaz, Y. Huang, L. Dai, Y. Li, M. Matthaiou, G. K. Karagiannidis, E. Björnson, K. Yang, I. Chih-Lin, and A. Ghosh, "Millimeter Wave Communications for Future Mobile Networks," *IEEE Journal on Selected Areas in Communications*, vol. 35, no. 9, pp. 1909–1935, Sept 2017.

[10] S. A. Busari, S. Mumtaz, K. M. S. Huq, J. Rodriguez, and H. Gacanin, "System-Level Performance Evaluation for 5G mmWave Cellular Network," in *GLOBECOM 2017 - 2017 IEEE Global Communications Conference*, Dec 2017, pp. 1–7.

[11] Claussen, "Efficient modelling of channel maps with correlated shadow fading in mobile radio systems," in *2005 IEEE 16th International Symposium on Personal, Indoor and Mobile Radio Communications*, vol. 1, Sept 2005, pp. 512–516.

[12] M. Rupp, S. Schwarz, and M. Taranetz, *The Vienna LTE-Advanced Simulators: Up and Downlink, Link and System Level Simulation*, 1st ed., ser. Signals and Communication Technology. Springer Singapore, 2016.

[13] N. Rupasinghe, Y. Kakishima, and . Gven, "System-level performance of mmWave cellular networks for urban micro environments," in *2017 XXXIInd General Assembly and Scientific Symposium of the International Union of Radio Science (URSI GASS)*, Aug 2017, pp. 1–4.

[14] A. H. Jafari, J. Park, and R. W. Heath, "Analysis of interference mitigation in mmWave communications," in *2017 IEEE International Conference on Communications (ICC)*, May 2017, pp. 1–6.

[15] F. Khan, Z. Pi, and S. Rajagopal, "Millimeter-wave mobile broadband with large scale spatial processing for 5G mobile communication," in *2012 50th Annual Allerton Conference on Communication, Control, and Computing (Allerton)*, Oct 2012, pp. 1517–1523.

[16] M. Shafi, A. F. Molisch, P. J. Smith, T. Haustein, P. Zhu, P. D. Silva, F. Tufvesson, A. Benjebbour, and G. Wunder, "5G: A Tutorial Overview of Standards, Trials, Challenges, Deployment, and Practice," *IEEE Journal on Selected Areas in Communications*, vol. 35, no. 6, pp. 1201–1221, June 2017.

[17] S. A. Busari, K. M. S. Huq, S. Mumtaz, L. Dai, and J. Rodriguez, "Millimeter-Wave Massive MIMO Communication for Future Wireless Systems: A Survey," *IEEE Communications Surveys Tutorials*, vol. 20, no. 2, pp. 836–869, Secondquarter 2018.

[18] Y. Liu, X. Fang, M. Xiao, and S. Mumtaz, "Decentralized Beam Pair Selection in Multi-Beam Millimeter-Wave Networks," *IEEE Transactions on Communications*, vol. 66, no. 6, pp. 2722–2737, June 2018.